ORIGINAL ARTICLE

Heating mechanism of the Abgarm–Avaj geothermal system observed with hydrochemistry, geothermometry, and stable isotopes of thermal spring waters, Iran

Abolfazl Rezaei[1,2] · Hadi Javadi[1] · Mahnaz Rezaeian[1,2] · Soghra Barani[1]

Abstract

In this study, the Abgarm–Avaj geothermal system in Iran is investigated by analyzing hydrochemistry and stable environmental isotopes of water samples collected from cold and thermal water springs and the Khare-Rud River together with tectonic settings. The findings reveal that the geothermal system is associated with the deep fault zone of Hasanabad and can be categorized into a convection dominated and non-magmatic geothermal system in accordance with the catalog of geothermal play types presented by Moeck (Renew Sustain Energy Rev 37:867–882, 2014). In fact, local rainfall that is occurred over the Kuhe-Bozorg limestone highlands percolates into a high depth along the main active fault of Hasanabad and then heats and emerges finally at the lowest topographic elevation of the fault in the form of thermal springs characterized by temperature ranges from 30 to 52 °C. The water samples from the thermal springs are of a high electrical conductivity value (ranges from 6585 to 11265 μS/cm) with the chloride water type. The lower circulation depth of meteoric water in the geothermal system is estimated to be about 3000 m by considering the possible maximum geothermal gradient of about 46 °C/km. The stable isotopes ratios analysis suggests that thermal water originates predominantly from rainfall occurring over the higher elevations, since the oxygen-18 ratios of the thermal spring waters are depleted than that of the cold spring waters. The equilibrium temperatures of the geothermal system are estimated via using the Na–K (Truesdell, Summary of section III: geochemical techniques in exploration. In: Proceedings of the 2nd U.N. symposium on the development and use of geothermal resources, vol 1. U.S. Government Printing Office, Washington, DC, pp liii–lxxx, 1976) and Na–K (Tonani, Some remarks on the application of geochemical techniques in geothermal exploration. In: Proceedings of advances in European geothermal research, 2nd symposium, Strasbourg, pp 428–443, 1980) geothermometers are 142–148 and 146–153 °C, respectively, which fall within the temperature range suggested by the mineral saturation indices (137–160 °C) and by the warm spring mixing model (135–164 °C) for the thermal spring waters. Furthermore, the results show that geothermal hot water mixes predominantly with shallow cold groundwater during ascending, where the portion of the cold shallow and deep-hot waters is about 70 and 30%, respectively.

Keywords Hydrothermal · Geochemistry · Geothermometry · Environmental stable isotopes · Abgarm–Avaj area · Hasanabad Fault · Iran

✉ Abolfazl Rezaei
    arezaei@iasbs.ac.ir; abolfazlrezaei64@gmail.com

    Hadi Javadi
    Javadih23@gmail.com

    Mahnaz Rezaeian
    m.rezaeian@iasbs.ac.ir

    Soghra Barani
    soghra@iasbs.ac.ir

1   Department of Earth Sciences, Institute for Advanced Studies in Basic Sciences (IASBS), Zanjan 45137–66731, Iran

2   Center for Research in Climate Change and Global Warming (CRCC), Institute for Advanced Studies in Basic Sciences (IASBS), Zanjan 45137–66731, Iran

Introduction

Employing geothermal systems for green production energy has been enhanced around the world significantly (Moeck 2014). Tester et al. (2007) claimed that it could technically supply 100,000 MW_{el} cost-competitive electric energy over the USA by 2050. In addition, thermal springs, as the main representative mark of geothermal systems, can play a major role in thermo-energetics for industrial use, balneology, health effect and recreational purposes, raw materials, and mineral supply (e.g., Miošić and Samardžić 2016; Modabberi and Yekta 2014). Thermal springs not only carry heat and fluids from deep reservoir to the surface, but also its hydrogeochemistry and isotopes ratios characteristics can provide valuable information about temperature, flow patterns, the origin of thermal fluids, and hydrogeological conditions of geothermal systems. Geochemical investigations of thermal waters have been widely applied in all stages of geothermal exploration and development (e.g., Giggenbach 1991; Mohammadi et al. 2010). Geochemical information should be interpreted in conjunction with geology, tectonic, and hydrogeological conditions of each area to lead to a reliable conceptual model for the geothermal system, since the conceptual model severely controls the successful development and production of the system. The prime geothermal systems are dominantly limited to the young volcanisms or tectonically active zones (Moeck 2014).

The Abgarm–Avaj area, located on the boundary between the main tectono-stratigraphic provinces of the Central Iran and the Sanandaj–Sirjan, consists of several thermal springs along the main active fault zones signifying the existence of a geothermal system. The area has also been detected as one of the potential geothermal areas in Iran by Yousefi et al. (2007).

In the work presented in this paper, we studied chemical and stable isotopes ratios of the cold and thermal spring waters and the Khare-Rud River in combination with tectonic settings to investigate (1) chemical and stable isotopes ratios of the thermal spring waters; (2) the percentage contribution of a shallow cold water mixed with ascending hot water via using the warm spring mixing model presented by Fournier and Truesdell (1974); (3) the equilibrium temperature of the system; and (4) heating mechanism of the geothermal system.

Geology and hydrogeology settings

The Abgarm–Avaj area is located in the Ghazvin Province, the western part of Iran (Fig. 1). Geodynamically, the area was formed as a result of both the northward convergence of the central Iran toward Eurasian and the northwestward movement of the South Caspian Basin related to Eurasia (Jackson et al. 2002; Ritz et al. 2006). Geologically, the area consists of two different tectono-stratigraphic provinces: the northern parts (i.e., Abgarm Region) are located in Central Iran, while the southern parts (i.e., Avaj area) placed in the Sanandaj–Sirjan zone, where the main fault of Avaj separated both zones (Figs. 1, 2). Recently, this active area has experienced several earthquake occurrences as a result of the high activity of the main fault zones of Avaj and Hasanabad (Alaei et al. 2017). The Avaj and Hasanabad faults, where interrupt different formations along the main geological structure and fold axes are the deep-seated old faults reactivated over the younger movements (Geological Survey of Iran 1978). The Hasanabad Fault, a long longitudinal, strike, and dip-slip fault (Geological Survey of Iran 1978), has a relative thick fractured zone, particularly near the thermal springs in the Abgarm Region (Fig. 2).

In the Abgarm Region, a wide range of stratigraphic units including Infra-Cambrian-to-Quaternary formations outcrops, whereas in the Avaj Region, they are dominantly metamorphic rocks of Jurassic-to-Quaternary sediments. As shown in Fig. 2, the main geologic units, in order of increasing age, are (1) Quaternary sediments (Q); (2) Miocene Upper Red formation, where consists of two units: URM (sandstone, marl, gypsum, and salt) and URC (conglomerate); (3) Oligo-Miocene Qom limestone formation (QF); (4) Eocene Karaj formation (KJF) which mostly consists of tuff and volcanic rocks; (5) Eocene Ziarat limestone formation (ZF); (6) Early Eocene Fajan conglomerate formation (FF); (7) The Cretaceous units of K1 (mainly limestone); (8) Jurassic Lar formation (LF), where consists of limestone with interbedded gypsum in some parts; (9) Jurassic Shemshak sandstone and shale formation (SHF); (10) Triassic Elika–Roteh carbonate formation (EF); (11) Permian Doroud–Ruteh formation which contains sandstone, shale, conglomerate, and limestone; (12) Cambrian Milla carbonate and shale formation (MF); (13) Cambrian Lalon sandstone formation (LAF); (14) Infra-Cambrian Barout formation (BF) which mainly consists shale, sandstone and dolomite; and (15) Infra-Cambrian Soltanieh dolomitic formation (SF).

A large amount of fresh groundwater in the area is related to the carbonate formations/units (e.g., K1 units and the Lar and Qom formations), where dominantly outcrop on the Kuhe-Bozorg highlands around the main fault of Hasanabad (Fig. 2). The evaporate-rich Upper Red formation outcrops widely in the area (Fig. 2), where severely degrades water quality. The Khare-Rud River which predominantly collects runoff produced over the evaporate-rich URM unit of the Upper Red formation is a saline river due to the dissolution of gypsum and salt beds of the URM. For example, the

Fig. 1 Study area and location of the water sampling points in the Abgarm–Avaj area. The coordinated system is the standard Universal Transverse Mercator UTM, World Geodetic System (WGS)
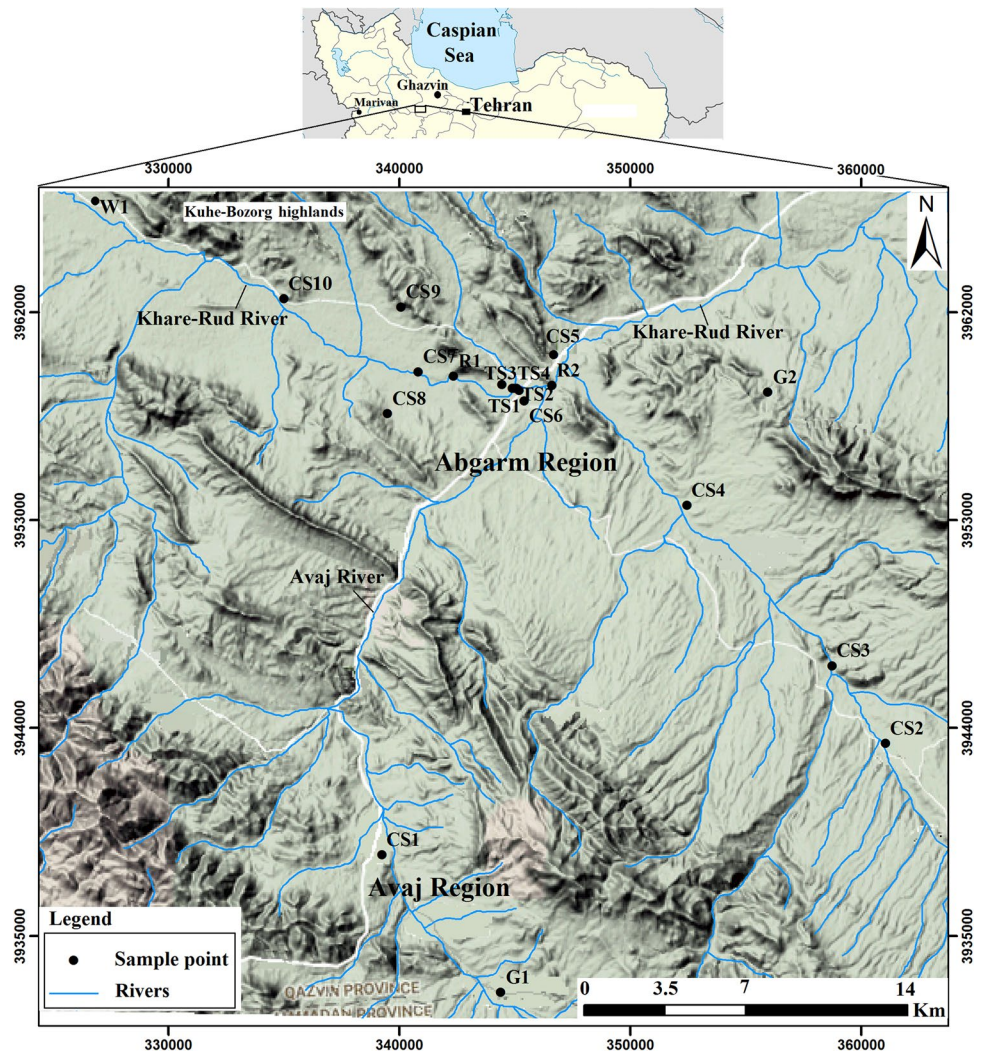
electrical conductivity (EC) at the sampling points of R1 and R2 taken from the river equals to 4150 and 2440 µS/cm, respectively.

The Abgarm Region is marked by several thermal springs (i.e., TS1–TS4) draining the Lar limestone formation along one of the main branches of the Hasanabad Fault near the Khare-Rud River. The Kherghan Spring (TS3) with a hot temperature (> 50 °C) is being used for balneology peruses as the main thermal spring of the area ($Q = 4$ l/s). The small thermal springs TS1 ($Q = 1$ l/s) and TS2 ($Q = 0.5$ l/s) emerge along the small fracture zones close to TS3. The EC and chemical characteristics of the thermal springs TS1–TS3 are the same. The thermal spring TS4 has a lower value of temperature (30 °C) and EC (6585 µS/cm). Since there is no indication of young volcanic activities, it seems that the geothermal system most probably is controlled by the main old deep-seated faults zones as well as the permeable limestone formations outcropped around the fault zone in the Kuhe-Bozorg highlands. In addition, both springs with the highest and lowest EC values in the area drain the Lar limestone formation. For instance, the cold spring CS9, characterized by EC of about 390 µS/cm and temperature of 16.65 °C, as well as all the thermal springs (TS1–TS4) having high values of EC (6585-11,265 µS/cm) and temperature (30–52 °C) emerge from the Lar formation. Note that the cold spring CS9 (1698 m) is located at a higher elevation than the thermal springs (~ 1550 m).

Method of study

The current investigation involves analyzing hydrochemistry and stable environmental isotopes (deuterium and oxygen-18) in water samples in conjunction with tectonic settings of the Abgarm–Avaj area to assess the geothermal system and to estimate the percentage contribution of deep-geothermal hot water in the thermal spring waters. We collected and analyzed water samples taken from Qanats (a gently sloping underground channel to drain groundwater to the surface), cold springs, thermal springs, the Khare-Rud River
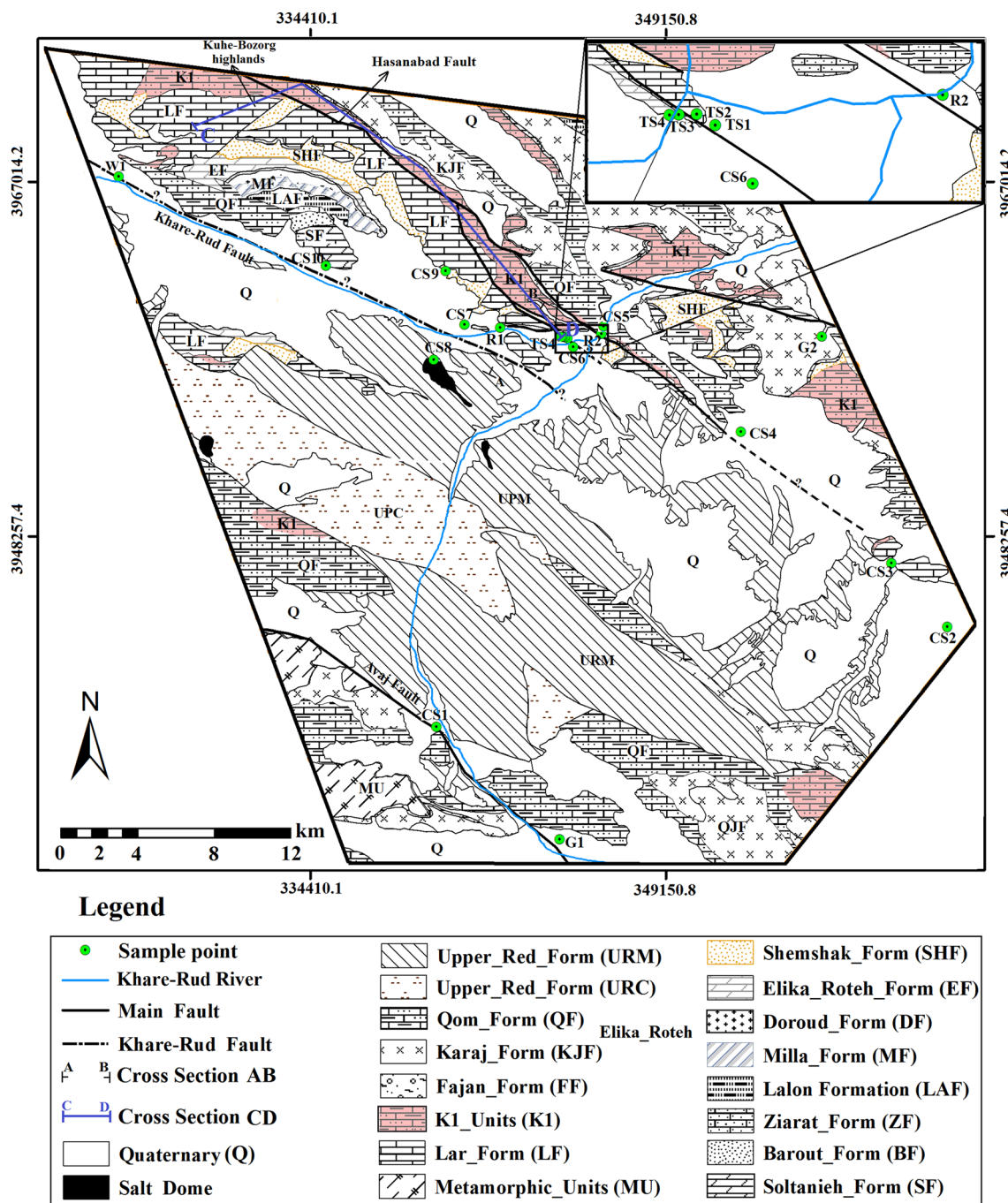
Fig. 2 Geology map of the Abgam–Avaj area with some hints on main rivers and location of sampling points overlain by a fault map. Symbols of CS and TS signify cold and thermal spring waters, respectively

and a production well. We collected two water samples, one in the early winter (January) and another in the late spring (June) 2017, from each sampling point for hydrochemical investigations. We tried to select the cold springs emerging from a different lithology as well as the cold springs are located nearby the thermal springs. The hydrochemical analysis results show that both the water samples which

were taken from each sampling point have approximately the same chemical characteristics; therefore, we used the average of physic-chemical parameter values observed in each water sampling point (Table 1).

We only collected one water sample from each sampling point to be analyzed for stable isotope ratios (deuterium and oxygen-18) in the late spring (June) 2017. Water

Table 1 Average of the physiochemical parameters of two different water samples taken from each sampling point (concentrations in mg/l)

ID	T (°C)	Q (l/s)	EC (μS/cm)	pH	Water type	Ca	Mg	Na	K	HCO₃	SO₄	Cl	Li	SiO₂	$\delta^2 H$ (‰)	$\delta^{18} O$ (‰)
G1	5.20	0.1	720	8.65	Ca–HCO₃	102	11.54	65	1.6	274	75	32	0.21			
G2	18.15	0.1	346.50	7.86	Mg–HCO₃	35	24.60	13	0.8	174	21	23	0.07			
CS1	14.60	2.5	934	7.98	Mg–HCO₃	55	59.54	48	8.6	409	34	110	0.21			
CS2	17.95	0.5	749.50	7.41	Mg–HCO₃	61	46.78	46	3.2	215	96	73	0.22			
CS3	12.75	105	1340	7.72	Na–HCO₃	73	40.70	117	5.4	329	197	168	0.33			
CS4	11.90	17	1106	7.25	Ca–HCO3	90	50.12	68	0.5	348	118	112	0.23			
CS5	17.40	90	2047	7.50	Na–Cl	138	35.84	275	9.34	357	195	456	0.44	16.6	-53.6 ± 0.6	-8.9 ± 0.2
CS6	17.25	16	1394	8.14	Na–Cl	56	49.82	186	5.4	232	112	420	0.28	8.9	-47.6 ± 1.1	-8.1 ± 0.3
CS7	13.35	0.2	3765	6.64	Na–Cl	145	51.64	450	14.5	432	343	843	0.68	14.6	-52.7 ± 1.1	-8.6 ± 0.2
CS8	15.90	0.3	643	7.89	Na–Cl	49	19.14	57	1.7	160	46	109	0.13			
CS9	16.65	2.4	390	8.00	Ca–HCO₃	52	14.88	17	1.7	159	19	48	0.09	8.1	-58.6 ± 1.1	-9.4 ± 0.5
CS10	16.60	2	2275	7.28	Na–Cl	151	42.22	271	7.3	479	153	488	0.38			
TS1	46.35	1	11,230	6.64	Na–Cl	402	126.66	1985	130.3	1673	368	4034	3.26	35.2		
TS2	44.40	0.5	11,265	6.77	Na–Cl	355	173.75	1939	125.4	1327	390	4038	3.26	35.3	-64.9 ± 1.6	-10.1 ± 0.2
TS3	53.10	4	11,240	6.85	Na–Cl	423	157.04	1954	130.4	1433	392	4006	3.26	35.2	-65.9 ± 1.9	-10.2 ± 0.3
TS4	30.85	2.7	6585	6.76	Na–Cl	298	65.00	970	60.5	875	343	2022	1.60	25.7	-59.2 ± 0.9	-9.6 ± 0.2
R1	16.40	–	4150	7.56	Na–Cl	110	109.35	371	14.5	216	280	1060	0.69			
R2	20.00	–	2440	7.50	Na–Cl	64	59.54	268	12.1	162	175	579	0.50			
W1	12.50	5	2060	7.72	Na–Cl	147	41.01	228	5.5	293	148	528	0.38			

The symbols of G, CS, TS, R, and W signify the Qanat, cold spring, thermal spring, river, and production well, respectively

samples (No 7) were taken from (1) the thermal springs TS2–TS4; (2) three cold springs CS5–CS7 which are supposed to be influenced by the geothermal system of the area in accord with the chemical results of the water samples taken in early winter; and (3) the cold spring CS9 emerging from the Lar formation as an end member of the cold groundwater in the area.

Applying the standard procedures, water samples were collected in clean plastic bottles for chemical analysis and in clean glass bottles for the stable isotopes ratios and then immediately sent to the geochemical lab. The water temperature, electrical conductivity (by Lovibond Conductivity-meter, SensoDirect Con 110), and pH (by Lovibond pH meter, SensoDirect pH 110) were measured in situ. Calcium and magnesium concentrations were determined using titration with EDTA (Eriochrom Black-T and Murexide as indicators). The flame photometry methods were used to measure the concentration of sodium, potassium, and lithium. Sulfate and silica concentrations were determined by spectrometry methods. Bicarbonate and chloride were measured using titration with H_2SO_4 (Methyl orange as the indicator) and silver nitrate (potassium chromate as the indicator), respectively. The stable isotope ratios of deuterium and oxygen-18 were determined using the high-precision laser spectroscopy by Mesbah Energy Company, Tehran, Iran. The results of chemical and stable isotopes ratios analysis and water type of the water samples are presented in Table 1.

Results and discussion

Water chemistry

As shown in Table 1, the water temperature ranges from 5.20 °C in the Qanat G1 to about 53 °C in the hot spring TS3. The pH ranges from 6.64 in the thermal spring TS1 to 8.65 in the cold Qanat G1. EC ranges from 346.5 μS/cm in the cold Qanat G2, characterized by the bicarbonate water type, to 11,265 μS/cm in the thermal spring TS2, with the chloride water type. The wide range of hydrochemistry characteristics in the area is due to various lithologies and complex hydrogeology conditions influenced by geothermal water.

The position of water samples on the Piper diagram is presented in Fig. 3, where the thermal springs fall in the corner of the region of the chloride water type (Fig. 3). The samples disperse somewhere between the cold spring CS9, the cold Qanat G2, and the thermal springs (TS1–TS4) on the Piper diagram as a result of various lithology and the influence of geothermal water. By considering the cold spring CS9, with the bicarbonate water type, as a cold water end member and the thermal springs as an end member of the thermal springs in the area, where they drain the Lar formation, we can conclude that the cold springs of CS5–CS7 and CS10 are influenced by the thermal water (Fig. 3). Notably, silica and lithium concentrations in the cold springs of CS5 and CS7 are greater than those in the other cold
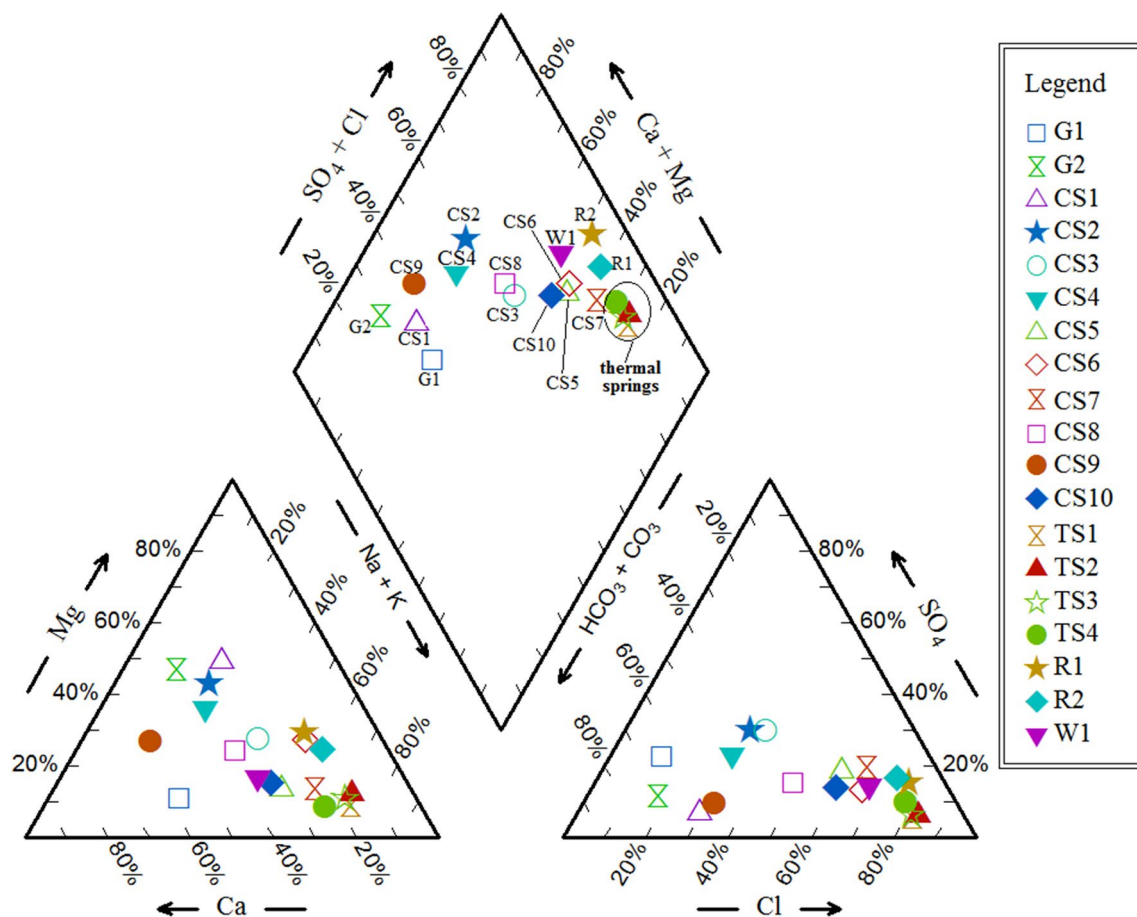
Fig. 3 Piper diagram of the water samples

springs such as CS9 (Table 1). As shown in Figs. 1 and 2, the cold springs CS5–CS7 is situated near the thermal springs, whereas the cold spring CS10 is located far away from the thermal springs. In addition, the cold springs of CS1–CS4 and CS8 as well as the cold water Qanats of G1 and G2 seem not be influenced by the geothermal water (Fig. 3). As shown in Fig. 2, the thermal springs as well as the cold springs affected by the thermal water are enclosed by the main faults of Hasanabad and Khare-Rud, whereas the cold springs CS1–CS4 and CS8 and Qanats G1 and G2 are situated outside of this zone. Notably, the cold spring CS1 and Qanat G1 are situated upon the main fault of Avaj implying that the geothermal system not related to the Avaj Fault.

The other notable point is that the water samples were taken from the Khare-Rud River (locations R1 and R2) and the production well (W1) have a chloride water type with very high EC. This is most probably due to the obvious effect of degrading water quality by the evaporative-rich unit of URM, not the geothermal waters, since (1) the Khare-Rud River upstream is also saline with a chloride water type (Afshar-Nia et al. 2016); (2) the production well (W1) is located near the Khare-Rud River (Fig. 2) and

its EC raises with increasing the water pumping over summer as a result of induced river recharge into the aquifer in which the well is drilled; (3) the river and well water samples plot close to each other on the Piper diagram (Fig. 3); and (4) while the thermal springs drain into the river somewhere between the locations of water samples R1 (upstream) and R2 (downstream), the water sample R1 has a higher EC than the water sample R2.

The saturation indices of anhydrate, chalcedony, gypsum, halite, and sepiolite minerals for all the samples are less than zero, implying that they are undersaturated in the groundwater of the area (Table 2). The saturation indices of aragonite, calcite, dolomite, and quartz minerals for all the thermal water springs (TS1–TS4) are higher than zero; thus, supersaturated. The values are reasonably corresponded to lithological settings of the area, since a most portion of groundwater system consists of carbonate rocks (e.g., Ziarat limestone, Cretaceous units of K1, Lar limestone, Elika carbonate, Milla, and Soltanieh formations). The super-saturation with respect to quartz may be due to high temperature as well as high-depth water circulation. In fact, the quartz concentrations in geothermal systems

Table 2 Saturation indices of anhydrate, aragonite, calcite, chalcedony, dolomite, gypsum, halite, quartz, and sepiolite minerals for the water samples

ID	Anhydrite	Aragonite	Calcite	Chalcedony	Dolomite	Gypsum	Halite	Quartz	Sepiolite
G1	− 2.11	1.17	1.33	–	1.74	− 1.57	− 7	–	–
G2	− 2.9	− 0.3	− 0.15	–	− 0.2	− 2.52	− 8	–	–
CS1	− 2.68	0.57	0.72	–	1.68	− 2.26	− 7	–	–
CS2	− 2.13	− 0.7	− 0.55	–	− 1	− 1.74	− 7	–	–
CS3	− 1.85	− 0.01	0.15	–	0.21	− 1.41	− 6	–	–
CS4	− 1.98	− 0.08	0.08	–	0.06	− 1.53	− 7	–	–
CS5	− 1.63	0.04	0.19	− 0.24	0.03	− 1.25	− 6	0.21	− 5.3
CS6	− 2.19	0.44	0.59	− 0.52	1.38	− 1.79	− 6	− 0.07	− 2
CS7	− 2.62	− 0.57	− 0.42	–	− 1	− 2.27	− 8	–	–
CS8	− 2.48	− 0.5	− 0.35	–	− 0.9	− 2.07	− 7	–	–
CS9	− 1.5	0.09	0.25	− 0.25	0.22	− 1.06	− 5	0.22	− 5.1
CS10	− 2.79	− 0.07	0.08	− 0.5	− 0.2	− 2.39	− 8	− 0.04	− 4.6
TS1	− 1.13	0.55	0.68	–	1.37	− 1.05	− 4	–	–
TS2	− 1.17	0.49	0.62	− 0.2	1.44	− 1.08	− 4	0.17	− 5.1
TS3	− 1.02	0.81	0.93	− 0.29	1.96	− 1.01	− 4	0.06	− 4.6
TS4	− 1.23	0.1	0.24	− 0.2	0.23	− 0.99	− 4	0.21	− 6.9
R1	− 1.69	0.06	0.21	–	0.65	− 1.29	− 5	–	–
R2	− 1.96	− 0.23	− 0.08	–	0.08	− 1.6	− 5	–	–
W1	− 1.76	− 0.04	0.11	–	− 0.2	− 1.32	− 6	–	–

usually are high as its solubility increases with increasing temperature.

A correlation matrix was calculated for all physiochemical parameters for the thermal springs (TS1–TS4) and the cold springs (CS5–CS7 and CS10) affected by the thermal water (Table 3). EC shows high correlation with ions of chloride, sodium, potassium, and lithium. These ions also show high correlations with each other. It, therefore, can be concluded that cations of sodium, lithium, and potassium are more appropriate for the cation geothermometry in the area in part due to that they have the highest correlation with the conservative ion of chloride as well as the concentrations of these ions are the highest in the thermal springs. Thus, it is expected that the sodium geothermometers (Na–K,

Na–K–Ca, and Na–Li) enable us to reasonably determine the equilibrium temperature of the reservoir.

The ternary diagram of Cl–SO_4–HCO_3 can be used to understand the maturity of geothermal systems (Giggenbach 1991). The mature water with neutral-chloride water type usually derives from a deep-hot geothermal system. The sulfate water type is often coming from geothermal steam-heated water influenced predominantly either by volcanic steam bearing high-temperature HCl or by geothermal steam bearing low-temperature H_2S (Dolgorjav 2009). The bicarbonate water type in the ternary diagram typically related to samples which are derived predominantly from meteoric water which is not intensively influenced by geothermal fluids. As outlined in Fig. 4, the thermal springs plot in the

Table 3 Correlation matrix of the physiochemical parameters in the thermal springs together with the cold springs of CS5–CS7 and CS10

	Temp	pH	EC	Ca	Mg	Na	K	HCO3	SO4	Cl	Li
Temp (°C)	1.00	–0.74	0.96	0.96	0.92	0.97	0.98	0.96	0.71	0.97	0.97
pH		1.00	–0.82	–0.89	–0.63	–0.79	–0.78	–0.82	–0.87	–0.78	–0.79
EC (uS/cm)			1.00	0.98	0.94	**1.00**	0.99	0.98	0.85	**1.00**	**1.00**
Ca (mg/l)				1.00	0.85	0.96	0.97	0.97	0.85	0.96	0.96
Mg (mg/l)					1.00	0.95	0.95	0.88	0.72	0.95	0.95
Na (mg/l)						1.00	**1.00**	0.99	0.81	**1.00**	**1.00**
K (mg/l)							1.00	0.99	0.78	**1.00**	**1.00**
HCO3 (mg/l)								1.00	0.79	0.98	0.98
SO4 (mg/l)									1.00	0.80	0.80
Cl (mg/l)										1.00	**1.00**
Li (mg/l)											1.00

The bold values are those parameters have a complete correlation with each other

Fig. 4 Ternary of Cl–SO$_4$–HCO$_3$ for water samples
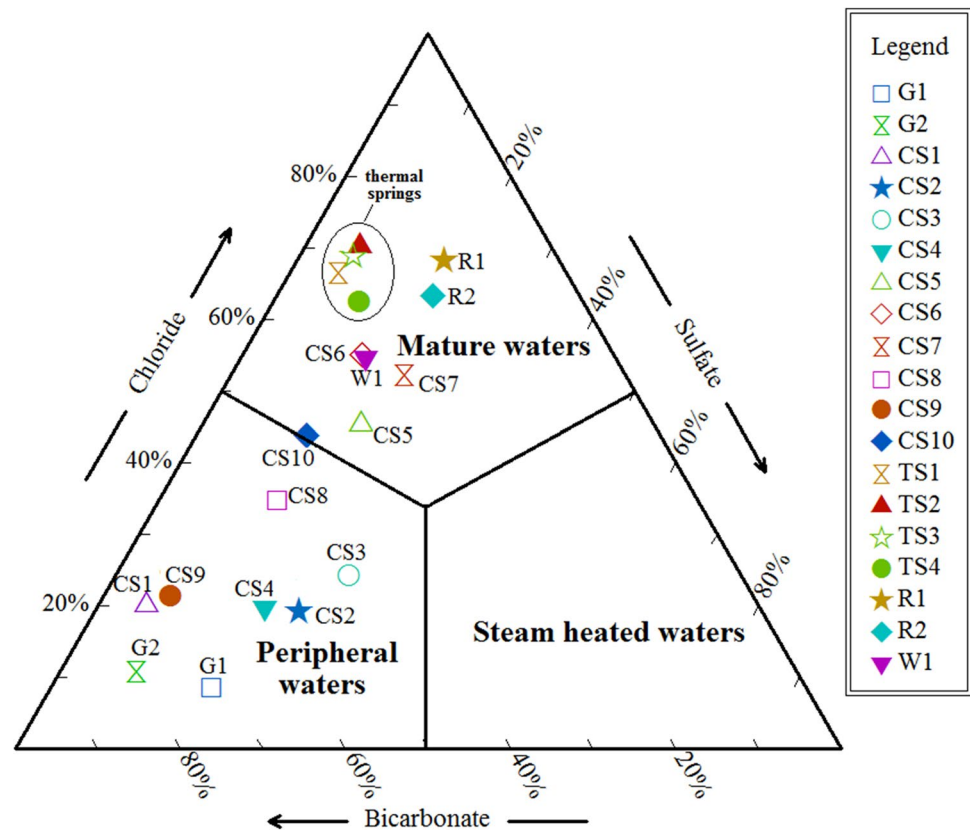
main field of mature waters, whereas no water sample falls in the steam-heated waters region, signifying that there is no any geothermal steam-heated water in the area (Dolgorjav 2009). Interestingly, the cold springs CS5–CS7 plot in the field of mature waters, where the cold spring CS10 falls near the mature-meteoric boundary. It signifies that thermal water influences the cold spring CS10 less than the cold samples of CS5–CS7. Over the map (Fig. 2), the cold spring CS10 is located far away from the thermal springs. The Qanats of G1 and G2 as well as the cold springs of CS1–CS4 and CS8 plot to the field of peripheral waters. The samples of R1, R2, and W1 plot to the field of mature waters. This is not due to the influence of the geothermal water, since its chemistry controls by the evaporate-rich URM unit contains gypsum and halite which have an effect of degrading water quality.

Stable isotopes

The stable isotope's ratios of oxygen-18 and deuterium in the Abgarm Region water samples together with the Mediterranean meteoric water line (MMWL), Iran meteoric water line (Iran MWL), Marivan meteoric water line (Marivan MWL), the city located in the western part of country at the same latitude as the study area (Fig. 1), and the best fit of the water samples in the area (notified as LMWL) are shown in Fig. 5. The maximum difference of oxygen-18 ratio

between the cold and thermal springs is only about 2‰ signifying that most probably all the cold and thermal springs have the same source. The main source seems to be rainfall which is occurred mainly during winter and spring upon the area. Interestingly, the stable isotope's ratios of the thermal spring waters are a little depleted than that of the cold spring waters. For example, the ratio of oxygen-18 in the hottest water spring TS3 (– 10.20‰) in the area is depleted than that of the cold spring CS9 (– 9.38‰), whereas both the springs drain the Lar limestone formation.

Notably, the LMWL plots around the Iran MWL and parallel to both the MMWL and Marivan MWL, signifying that groundwater (both the thermal and cold springs) of the area originates from local precipitation. Precipitation occurrence over Iran, particularly in western parts, comes predominantly from the Mediterranean Sea (Alijani and Harman 1985; Raziei et al. 2012). In fact, a small quantity of evaporation, boiling, rock exchange, or mixing can affect stable isotopes ratios in the spring's water (Powell and Cumming 2010). In general, the cold springs emerge at the higher elevations of the area are more depleted in oxygen-18 ratio, where the ratio in water of the springs of CS9 (1700 m), CS7 (1595 m), and CS6 (1571 m) is − 9.38, − 8.58, and − 8.15‰, respectively.

Considering the above-mentioned, it can be concluded that the thermal springs mainly originate from local
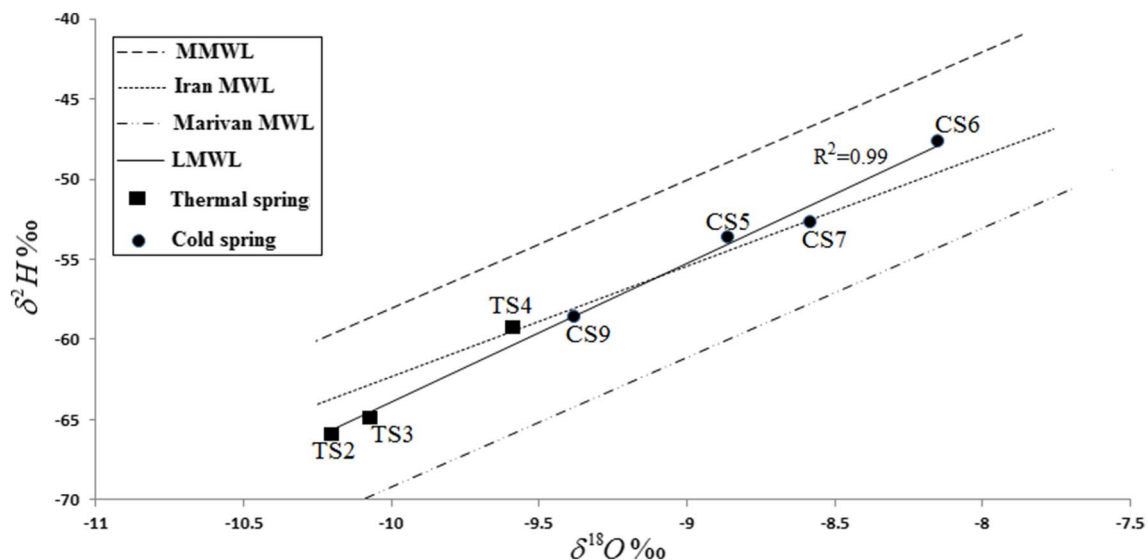
Fig. 5 Stable isotopes content of the water samples together with the Mediterranean meteoric water line, MMWL ($\delta D = 8\delta^{18}O + 22$), Iran meteoric water line, Iran MWL ($\delta D = 6.89\delta^{18}O + 6.57$, Shamsi and Kazemi 2014) and Marivan meteoric water line, Marivan MWL ($\delta D = 8.07\delta^{18}O + 11.5$, Shamsi and Kazemi 2014) and the local meteoric water line obtained from the best fit of the springs, LMWL ($\delta D = 8.65\delta^{18}O + 22.55$).

precipitation occurs at higher elevations in comparison with the cold springs of CS5–CS7 and CS9. Rainfall may percolate into the underground system at the limestone outcrops at the Kuhe-Bozorg highlands along the Hasanabad Fault. It is, therefore, expected that the deep fault zone of Hasanabad is of high permeability and hence allows water to percolate into high depth. Its high permeability may be due to that majority of the formations interrupted by the Hasanabad Fault to high depth are fractured carbonates (mainly limestone) and sandstone. The carbonate rocks have a high permeability as a result of its high intrinsic solubility as well as its high potential of structural fracturing. In fact, there is a high thermal gradient along the high permeable deep fault zones (Tanaka et al. 2007). Consequently, we can conclude that the Hasanabad Fault zone may have not only a high permeability but also a high thermal gradient. It is indicated that the Moho boundary beneath the area is located at the shallower depth in comparison with the Zagros (to the southern parts) and Alborz (to the northern parts) areas (e.g., Chen et al. 2016; Motaghi et al. 2017).
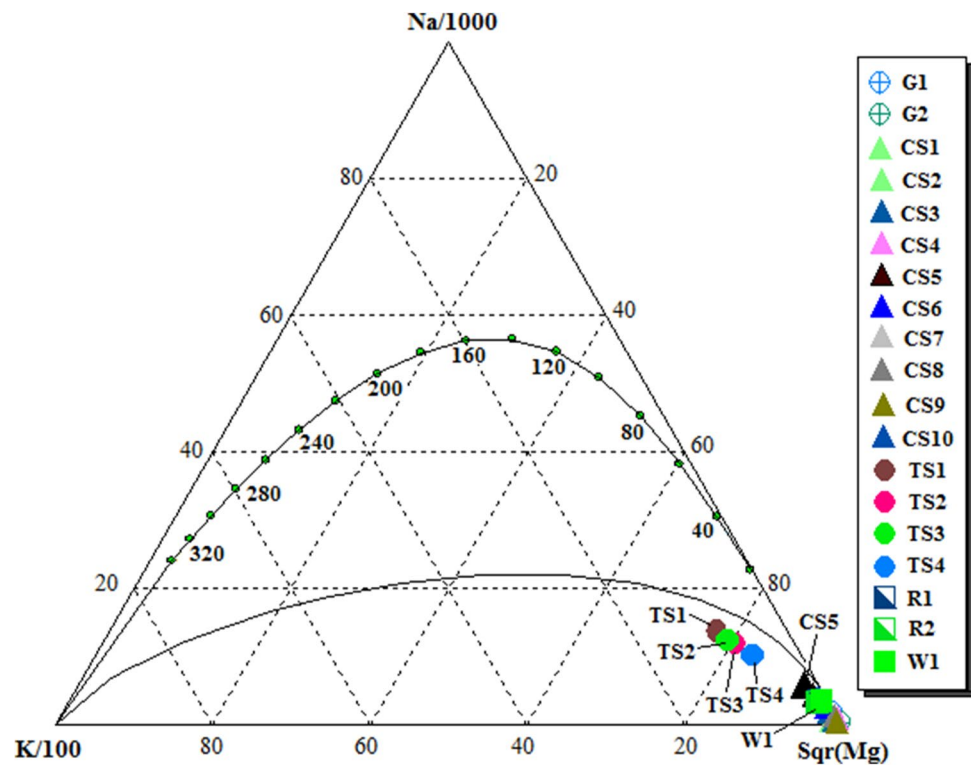
The equilibrium temperature of the geothermal system

The Na–K–Mg ternary diagram obtained by Giggenbach (1988) is commonly used to select appropriate water samples for geothermometry (Strelbitskaya and Radmehr 2010). As can be seen in Fig. 6, all samples plot in the immature field, where the thermal springs are separated from the cold waters and plot near the boundary of immature-partial equilibrium.

Nevertheless, none of the thermal springs have reached full equilibrium with host rocks of the reservoir. Hence, we tried to evaluate the equilibrium temperature of the system using (1) both silica and cation geothermometers; (2) the state of mineral saturation indices at different temperatures using the thermal spring waters; and (3) the warm spring mixing model presented by Fournier and Truesdell (1974).

Chemical geothermometry

The chemical geothermometers such as silica, Na–K, Na–K–Ca, Na–K–Ca–Mg, Mg–Li, and Na–Li have been used extensively to assess the equilibrium temperature in geothermal reservoirs (Fournier and Truesdell 1973; Giggenbach 1988; Karimi et al. 2017; Kharaka and Mariner 1989; Mohammadi et al. 2010). Here, we attempted to estimate the equilibrium temperature of the reservoir using different silica and cations geothermometers. The average temperatures estimated by both the silica (quartz and chalcedony) and cation (Na–K, Na–K–Ca, and Na–Li) geothermometers are listed in Table 4. The temperature values obtained by the chalcedony geothermometer are not true as the values approximately equal to the temperature observed in the hottest spring water TS3 (~52 °C). The equilibrium temperature estimated from the thermal spring waters ranges from 94 to 108 °C using the quartz geothermometer which seems to be underestimated in comparison with the temperature values estimated by the sodium geothermometers (Na–K, Na–K–Ca, and Na–Li), mineral saturation indices and the warm spring mixing model which are presented in the

Fig. 6 Giggenbach ([1988](#)) diagram for the water samples

Table 4 Equilibrium temperature of the Abgarm–Avaj geothermal system estimated by the different geothermometers

ID	Spring Temp. (°C)	Na–K				Na–K–Ca (Fournier and Truesdell 1973)[e]	Na–Li (Kharaka and Mariner 1989)[f]	Quartz (Fournier 1977)[g]	Chalcedony (Fournier 1977)[h]
		Truesdell (1976)[a]	Fournier (1977)[b]	Tonani (1980)[c]	Arnórsson et al. (1983)[d]				
CS5	17	95	< 150	97	115	66	171	57	24
CS6	17	84	< 150	86	105	63	167	35	3
CS7	13	91	< 150	94	112	84	169	52	20
TS1	46	146	183	151	168	175	173	86	55
TS2	44	145	182	150	166	175	174	86	55
TS3	53	148	185	153	169	175	174	86	55
TS4	31	142	180	146	163	163	174	73	41

[a] $T = 855.6/(0.8573 + \log[\text{Na}/\text{K}]) - 273.15$

[b] $T = 1217/(1.483 + \log[\text{Na}/\text{K}]) - 273.15$

[c] $T = 833/(0.780 + \log[\text{Na}/\text{K}]) - 273.15$

[d] $T = 933/(0.933 + \log[\text{Na}/\text{K}]) - 273.15$

[e] $T = 1647 \Big/ \left(2.47 + \log[\text{Na}/\text{K}] - \beta[\log\left(\sqrt{\text{Ca}}/Na\right) + 2.06]\right) - 273.15, \beta = 4/3 \text{ if } T < 100\,°C, \beta = 1/3 \text{ if } T < 100\,°C$

[f] $T = 1590/(0.779 - \log[\text{Na}/Li]) - 273.15$

[g] $T = 1309/(5.19 - \log[SiO_2]) - 273.15$

[h] $T = 1032/(4.69 - \log[SiO_2]) - 273.15$

following sections. It may be due to that the silica geothermometers intensively influence by boiling and dilution more than the cation geothermometers (Davraz [2008](#)). Fournier and Truesdell ([1974](#)) suggested that the silica geothermometers should be used with caution for geothermometry at

the spring temperature. The temperature values obtained using the Na–K–Ca–Mg (> 350 °C) and Mg–Li (< 93 °C) geothermometers are incorrectly overestimated and underestimated, respectively (not listed in Table [4](#)). It, therefore, can be concluded that the magnesium geothermometers are not

appropriate in the area may be due to that the magnesium is intensively influenced by mixing and cation exchange within the system (Davraz 2008). Notably, the mixing model, presented in section of "Warm spring mixing model", is indicated that the hot water is mixed with the cold shallow water during ascending.

However, temperatures estimated using the Na–K (Fournier 1977) and Na–K–Ca geothermometers for the thermal spring waters (TS1–TS4) range from 180 to 185 and 163–175 °C, respectively. Notably, the temperature obtained from the Na–Li geothermometer is equal to about 174 °C for the thermal spring waters and 167–173 °C for the cold spring waters. It can be seen that the temperature ranges estimated by these three cation geothermometers are approximately equal and the values in the different thermal springs do not show sharp variations, particularly in the case of the Na–Li geothermometer. In addition, we estimated the temperature using Na–K (Truesdell 1976), Na–K (Tonani 1980), and Na–K (Arnórsson et al. 1983) and the value ranges of 142–148, 146–153, and 163–169 °C obtained, respectively. The values obtained from the Na–K (Truesdell 1976), Na–K (Tonani 1980) are approximately the same and in both the temperature ranges suggested by the mineral saturation indices (137–160 °C) and by the warm spring mixing model (135–164 °C) in the following sections.

Mineral saturation indices at different temperatures

Mineral-solution equilibrium, i.e., saturation index (SI) at a wide range of temperature, is an alternative approach to calculate the equilibrium temperature of geothermal systems, particularly in the case that thermal water samples fall in the immature field on the Na–K–Mg ternary diagram (Gökgöz and Tarcan 2006; Reed and Spycher 1984). SI of water samples was estimated at different minerals by the PHREEQC code (Parkhurst and Appelo 1999). One can write SI as follows:

$$SI = \left(\log \frac{IAP}{K_T} \right), \tag{1}$$

where IAP is the ion activity product and K_T signifies the mineral equilibrium constant at the water temperature. For $SI = 0$, the mineral and its surrounding water are in full equilibrium condition. $SI < 0$ and $SI > 0$ signify the sub-saturation and super-saturation conditions, respectively. In fact, to observe how SI of each mineral change with temperature for a particular chemistry characteristic measured in each sampling point, the diagram of SI versus temperature for different minerals is plotted (such as Fig. 7). Then, if a group of minerals has SI values close to the equilibrium condition (i.e., $SI \approx 0$) at a similar temperature, this temperature range can be considered as an equilibrium temperature range in the reservoir.

The SIs of anhydrite, calcite, dolomite, quartz, sepiolite, chalcedony, and gypsum in the thermal spring waters of TS2 and TS3, as a representative of the thermal waters of the area, are presented in Fig. 7. As can be seen in Fig. 7, the thermal springs of TS2 and TS3 suggest two different equilibrium temperature ranges: 103–120 °C resulted from the intersection of anhydrite, quartz, and chalcedony curves and 137–160 °C at the intersection of quartz, sepiolite, chalcedony, and gypsum curves. It seems that the latter (137–160 °C) is more reasonable due to it is (1) resulted from the intersection of four different mineral curves and (2) close to the equilibrium temperature ranges suggested by the warm spring mixing model and sodium geothermometry. Calcite and dolomite minerals do not cross the line of equilibrium condition (i.e., $SI \approx 0$). Nevertheless, if we considered that the cross point of calcite and dolomite can also represent the equilibrium temperature, then the upper limit of the equilibrium temperature in the system is about 185 °C.
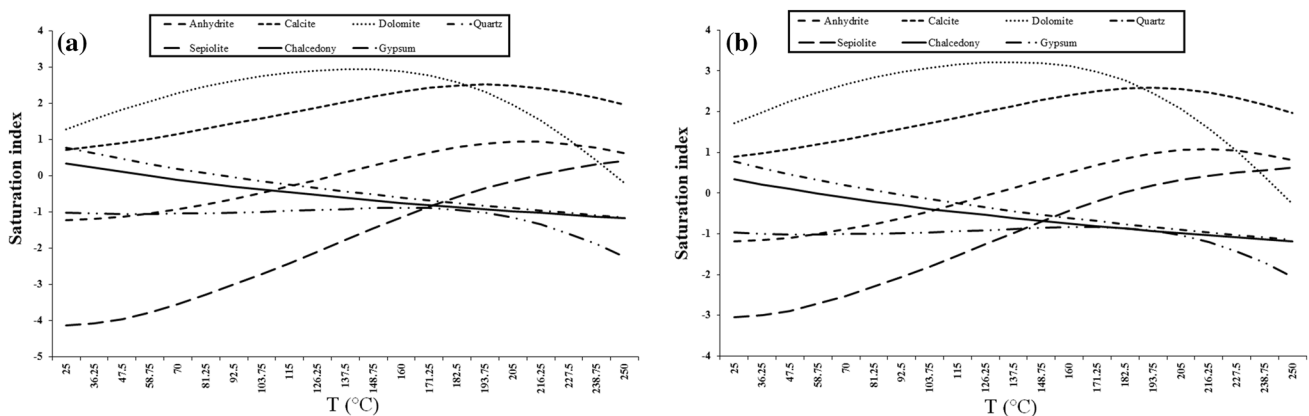

Fig. 7 Mineral saturation indices (SIs) versus temperature (range from 25 to 250 °C) in the thermal springs of **a** TS2 and **b** TS3

Warm spring mixing model

To assess the equilibrium temperature of the system, we also used the warm spring mixing model which has been applied previously by different researchers (e.g., Arnorsson 1985; Fournier and Truesdell 1974; Mohammadi et al. 2010). The ascending hot water is diluted predominantly by shallow cold groundwater and its temperature drops down depends on temperature and fraction of hot water mixed with cold shallow water. The warm spring mixing model tries to evaluate the fraction of cold water mixed with the ascending thermal water using the temperature and silica values measured in a warm thermal spring (< 80 °C) and in a cold spring which is not influenced by the geothermal fluids (Fournier and Truesdell 1974). Fournier and Truesdell (1974) presented two different models, where the model one works truly in the cases that the warm springs are not the result of steam mixing with the cold waters like our case. In our case, there is no any fumarole in the area as well as none of the thermal springs plot to the steam-heated region in Fig. 4, implying no existence of steam mixing with cold waters. The model one uses two equations to obtain two unknowns of (1) temperature of original hot water and (2) fraction of cold shallow water mixed with the ascending hot water. The second equation is as follows (Fournier and Truesdell 1974):

$$H_{\text{cold}} \times X + H_{\text{hot}} \times (1 - X) = H_{\text{spring}}, \qquad (2)$$

where H_{cold}, H_{hot}, and H_{spring} are the heat contents or enthalpies of the cold end-member spring, the original hot water, and the warm spring, respectively, and X and $1–X$ represent the proportion of cold spring and of original hot water, respectively.

Similarly, the third equation is written as

$$Si_{cold} \times X + Si_{hot} \times (1 - X) = Si_{spring}, \qquad (3)$$

where Si_{cold}, Si_{hot}, and Si_{spring} are the silica contents of the cold end-member spring, the original hot water, and the warm spring, respectively. Fournier and Truesdell (1974) presented a five-stage graphical procedure to solve the equations to obtain the unknowns. One can find the detailed procedure of the solution presented in the works by Fournier and Truesdell (1974). Finally, a graph like that of Fig. 8 is obtained for each warm spring in which the cross point of the silica and enthalpy curves represents both the equilibrium temperature of the hot water and the faction of the cold water mixed with the hot water to emerge from the warm spring. As can be seen in Fig. 8, the thermal spring waters of TS1–TS3, as a representative of the thermal water in the area suggest the equilibrium temperature of the system to range from 140 to 164 °C which falls in the range estimated by the mineral saturation indices (137–160 °C). Note that Fig. 8d was obtained using silica concentration (31.8 mg/l)

and water temperature (~ 50 °C) measured by Zamani et al. (2013) at the location of the thermal spring TS3. The temperature value (~ 137 °C) obtained from the thermal spring TS3 (both Fig. 8c, d) may be more reasonable than those from other thermal springs, since its surface temperature (~ 52 °C) and discharge (4 l/s) are higher than those of the thermal spring waters TS1 (46.35 °C and 1 l/s) and TS2 (44.4 °C and 0.5 l/s). The thermal spring TS1 is a small fractured spring along a small fractured zone near the spring TS3. The small thermal spring TS2 was emerged near to the thermal spring TS3, and about 2 years ago, some parts of the limestone of the area were cut for building a new swimming pool. This spring is draining thermal water along a dissolution fracture through limestone rocks of the Lar formation. It seems that both the thermal spring waters TS1 and TS2 are more cooled by conduction occurred near the land surface, since their chemical and stable isotopes characteristics are the same as those from the thermal spring TS3. Therefore, we believed that the equilibrium temperature and percentage contribution of cold water obtained using the warm spring mixing model for the water sample TS3 are more reasonable, since this mixing model severely depends upon the spring temperature.

The contribution of shallow cold groundwater was obtained to be about 70%. On one hand, the total discharge rate of original hot water emerges from the thermal springs TS1–TS3 is about 1.65 l/s which is diluted by about 3.9 l/s of cold water. The total discharge rate of the thermal springs TS1–TS3 is about 5.5 l/s. On the other hand, it signifies that the recharge may occur only along a narrow route like the main fault zone. The lower circulation depth of meteoric water recharged into the geothermal system was estimated to be about 3000 m by considering the average equilibrium temperature of about 137 °C [average of TS3 and TS3 (2013) in Fig. 8c, d] and the maximum thermal gradient of the intraplate continental crust (46°C/km), reported by Sutherland et al. (2017). However, it seems that the lower circulation depth may be more than 3000 m as the thermal gradient is most probably less than 46°C/km.

The heating mechanism of geothermal water

To clarify the movement mechanism of geothermal fluids in the Abgarm–Avaj area, we examined the stable isotope's ratios of the spring waters, the distribution of the cold springs, particularly those are influenced by the thermal waters, the equilibrium temperature of the reservoir estimated above, geology settings, and the location of the main active faults in the area.

The evidence shows that the geothermal system is not related to volcanic activities in part due to that (1) lack of any young volcanic activity around; (2) none of the thermal springs plot in the steam-heated region in the $Cl–SO_4–HCO_3$
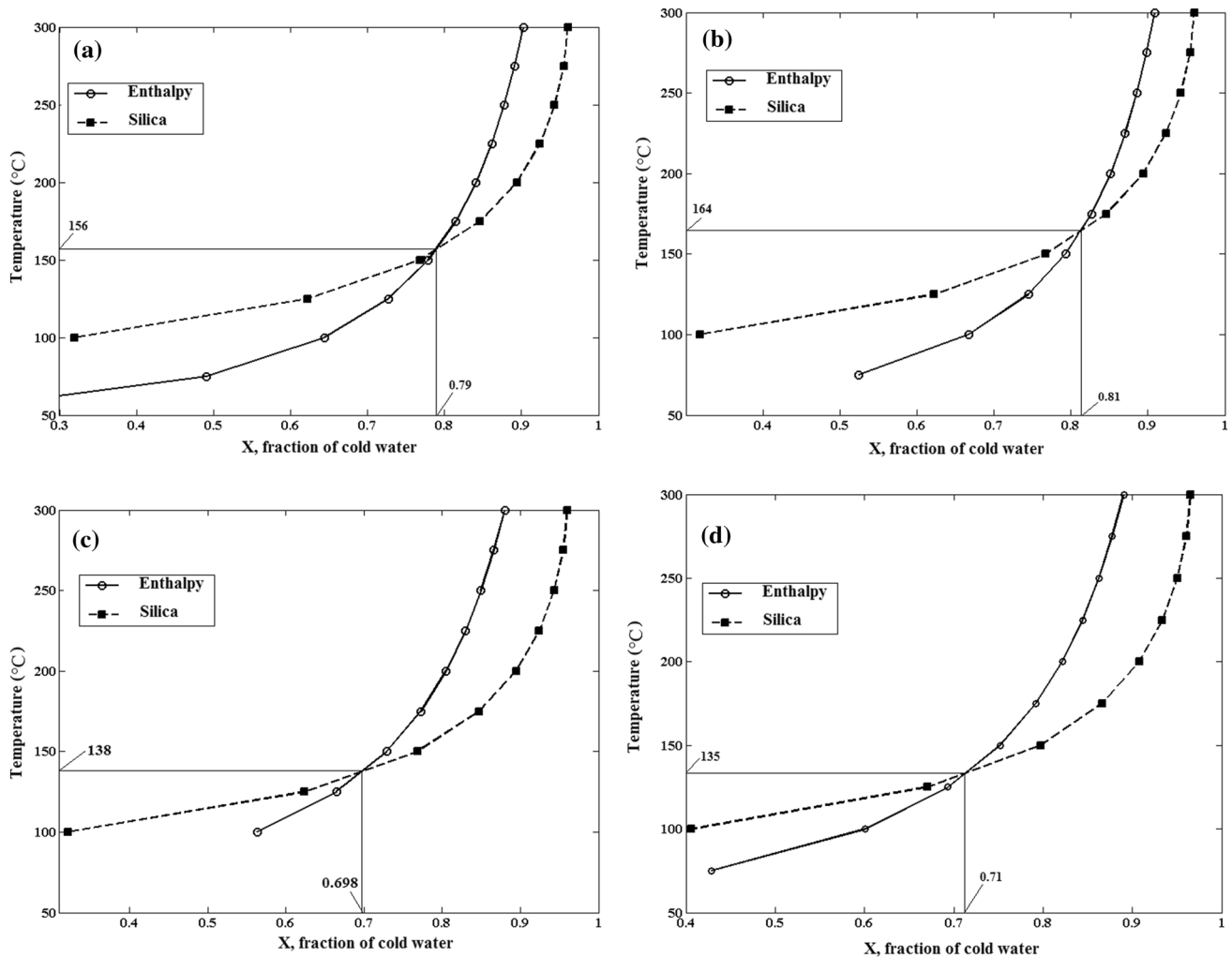
Fig. 8 Fraction of cold water mixed with the hot water versus temperature of the geothermal system using **a** TS1, **b** TS2, **c** TS3, and **d** TS3 (2013)

ternary diagram (Fig. 4); and (3) not only enrichment in the oxygen-18 ratio does not occur in the thermal spring waters, but also its oxygen-18 ratio is depleted than that for the cold spring waters. The geothermal system appears to be in relation with the main active deep-seated faults of the area, particularly the Hasanabad Fault. The Hasanabad Fault goes through the high-elevation parts of the area (the Kuhe-Bozorg highlands) towards the lowest elevation parts of the area (the Khare-Rud River and the thermal spring locations), as shown in Fig. 2. It is a main active fault with several branches which transects mainly the carbonate formations with the large permeability not only at the Kuhe-Bozorg highlands with a high quantity of snowfall annually, but also over the deep depth (Figs. 9, 10). Note that limestone beds, particularly, the Lar formation and the K1 units, outcrop widely at the Kuhe-Bozorg highlands around the Hasanabad Fault. In fact, the Hasanabad Fault crosses difference ranges of topography elevation from about 2550 m,

at the Kuhe-Bozorg highlands to 1550 m, at the location of the thermal springs (Figs. 1, 10). In reality, the relief difference between the highland and the thermal spring locations is about 1000 m. With considering the above-mentioned points, the hypothesis is that the Hasanabad Fault system allows meteoric water to conventionally percolate into high depth, heats and then ascends back to the surface along the active fault zone as a result of convection of the regional groundwater flow, as shown in Fig. 10 (Hochstein et al. 2013). The main reasons confirm the hypothesis including (1) all the thermal springs emerge along one of the main branches of the Hasanabad Fault when it crossing the Khare-Rud River at the lowest elevation of the fault branches (Figs. 2, 10); (2) the cold springs (CS5–CS7 and CS10) affected by the geothermal water are dispersed near the thermal springs, particularly around the main fault of Hasanabad (Fig. 2); and (3) the stable isotope's ratios of the thermal spring waters is depleted than of the cold spring

Fig. 9 Geological cross section near the thermal springs of the Abgarm Region across the main faults of Hasanabad and Khare-Rud. The location of the cross section (AB) is shown in Fig. 2. The lithological symbols are those presented in Fig. 2. Modified from Geological Survey of Iran (1978)
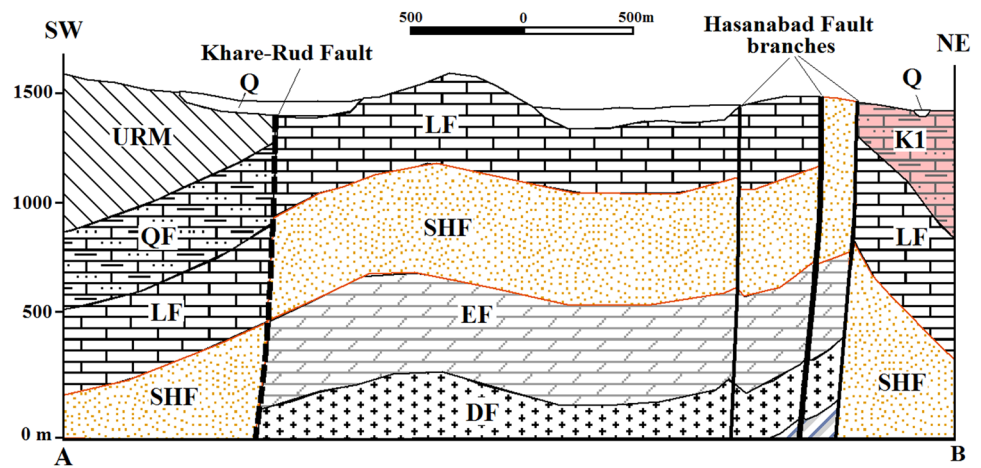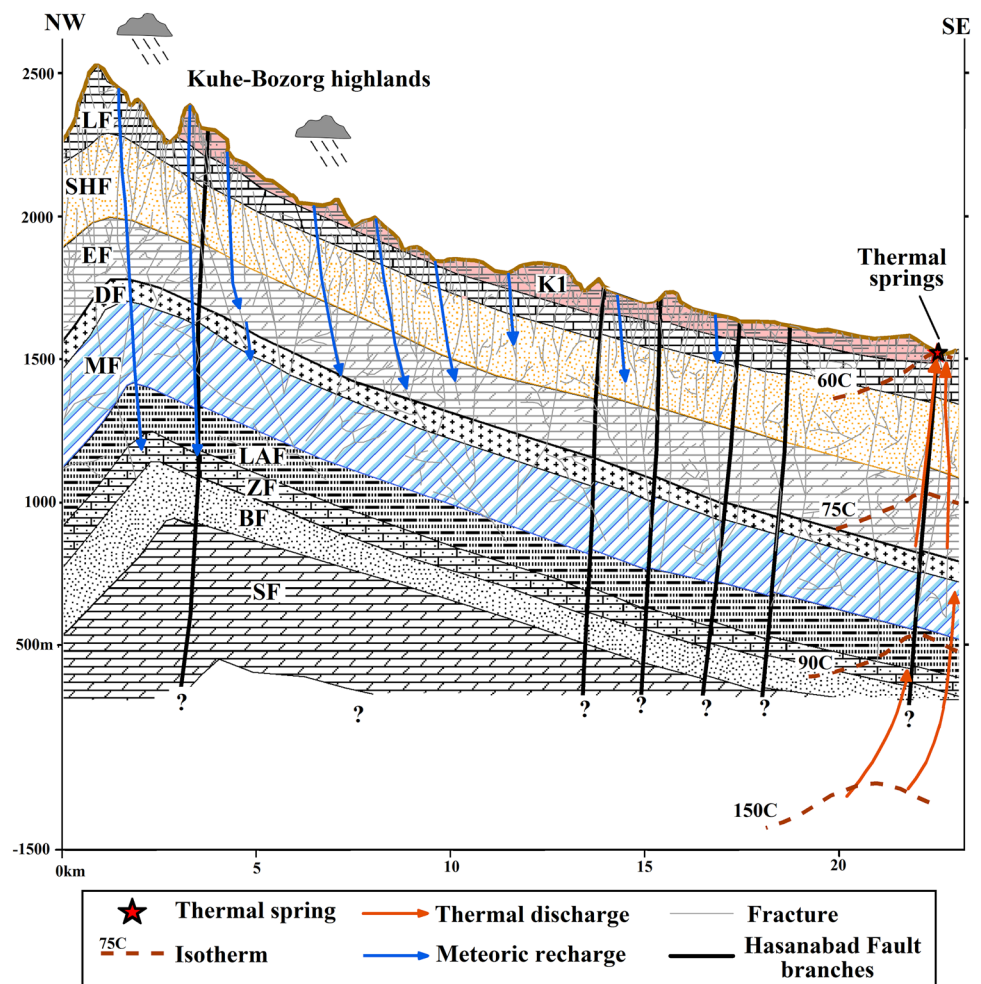

Fig. 10 Simple schematic conceptual model of the heating mechanism from the Kuhe-Bozorg highlands to the location of the thermal springs in the Abgarm Region. The location of the cross section (CD) is shown in Fig. 2. The lithological symbols are those presented in Fig. 2

waters (Fig. 5). In fact, in a specific region, the depleted stable isotopes originates from meteoric water occurred on higher elevations (Clark and Fritz 1997).

As shown in the conceptual model of Fig. 10, it seems that local rainfall occurs over the karstic limestone rocks (Lar formation and the Cretaceous units of K1) in the Kuhe-Bozorg highlands percolates along the main active fault of Hasanabad to a high deep depth and is heated by geothermal gradient. Subsequently, the hot water ascends along the Hasanabad Fault branches and emerges at the lowest topographic elevation of the fault in the Abgarm Region. In fact, the deep fault system provides fractured permeable

zones mainly consists of carbonate and sandstone (Figs. 9, 10) allowing the water to percolate into the deeper layers, heated and then ascends predominantly along the Hasanabad Fault branches. Notably, most of the famous geothermal fields around the world consist of carbonate (e.g., Bavarian Molasse Basin) and sandstone (e.g., North German Basin and central part of Alberta Basin), as listed by Moeck (2014).

According to the catalog of geothermal play types presented by Moeck (2014), the Abgarm-Avaj geothermal system seems to be categorized into the convection dominated and non-magmatic geothermal plays, since (1) it is located near the convergent settings of Arabian–Eurasian plates and linked with a high topographic relief; (2) the estimated temperature of the Abgarm–Avaj geothermal system (about 135–185 °C) is fallen in the range of moderate temperature ($150 \pm 30\ ^{O}C$) presented by Moeck (2014) for this type of fault-controlled geothermal systems; (3) most probably, the convection occurs along the main fault of Hasanabad, where along it the main recharge (the Kuhe-Bozorg highlands) and discharge (around the thermal springs TS1–TS4) zones are dispersed (Figs 9 and 10); (4) rainfall occurs over the Kuhe-Bozorg highlands is the main source of the thermal springs; (5) the thermal spring waters are of a high-Cl water type; and (6) the Moho boundary beneath the area is located at the shallower depth in comparison with the zones of Zagros and Alborz (Chen et al. 2016; Motaghi et al. 2017).

Conclusions

The current study investigates the Abgarm-Avaj geothermal system, Iran. It was carried out by analyzing hydrogeochemistry and stable isotopes in conjunction with tectonic settings. The thermal water, with a Na–Cl water type, derives from meteoric water with a lower circulation depth of about 3000 m along the main active fault of Hasanabad, where is recharged mainly through the limestone Kuhe-Bozorg highlands (mainly the Lar formation and K1 units). None of the springs along the main fault of Avaj is influenced by the geothermal water. The stable isotopes ratios (deuterium and Oxygen-18) in the thermal spring waters is depleted than that of the cold spring waters signifying that the local rainfall occurs at high-elevated highlands is the main source of the thermal waters. The thermal springs were categorized as immature water based on the Na–K–Mg ternary diagram. Totally, the equilibrium temperature of the reservoir was estimated to range from 142 to 148, 146–153, 137–160, and 135–164 °C using Na–K geothermometer presented by Truesdell (1976) and Tonani (1980), mineral saturation indices and the warm spring mixing model, respectively. The warm spring mixing model also suggests that hot water mixed with shallow cold meteoric water during ascending,

since the portion of cold shallow and hot waters is about 70 and 30%, respectively. Hence, the silica geothermometers are underestimated the real equilibrium temperature of the system. Moreover, some number of the cold springs located near the thermal springs, particularly around the Hasanabad Fault zone, are influenced by the geothermal water, while the chemistry of the Khare-Rud River controls predominantly by the evaporate-rich Upper Red formation outcrops widely over the river catchment area.

The results of the study can be applied to the future geothermal energy development in the Abgarm–Avaj area which is planning by the Renewable Energy Organization of Iran (SANA).

References

Afshar-Nia M, Khodabakhsh S, Rafiei B, Momen-Alizadeh A (2016) Zonation of the Khar-rud River (south Qazvin Province) based on the water type and its relation with saline formations. In: 10th International river engineering conference, Shahid Chamran Univeristy, 16–26 Jan 2016, Ahwaz

Alaei M, Dehbozorgi M, Ghassemi MR, Nozaem R (2017) Evaluation of relative tectonic activity of Buin Zahra–Avaj area, northern Iran. Arab J Geosci 10(10):229

Alijani B, Harman JR (1985) Synoptic climatology of precipitation in Iran. Ann Assoc Am Geogr 75(3):404–416

Arnorsson S (1985) The use of mixing models and chemical geothermometers for estimating underground temperatures in geothermal systems. J Volcanol Geotherm Res 23:235–299

Arnórsson S, Gunnlaugsson E, Svavarsson H (1983) The chemistry of geothermal waters in Iceland. III. Chemical geothermometry in geothermal investigations. Geochim Cosmochim Acta 47:567–577

Chen L, Jiang M, Talebian M, Ghods A, Chung SL, Ai Y, Faridi M (2016) New seismic array observation in the Northwestern Iranian Plateau. In: EGU general assembly conference abstracts, vol 18, p 3427

Clark ID, Fritz P (1997) Environmental isotopes in hydrogeology. LEWIS PUBLISHERS, Boca Raton, 352 p

Davraz A (2008) Hydrogeochemical and hydrogeological investigations of thermal waters in the Usak Area (Turkey). Environ Geol 54(3):615–628

Dolgorjav O (2009) Geochemical characterization of thermal fluids from the Khangay area, Central Mongolia. Geothermal training programme reports, Orkustofnun, Grensásvegur, p 9

Fournier RO (1977) Chemical geothermometers and mixing models for geothermal systems. Geothermics 5(1–4):41–50

Fournier RO, Truesdell AH (1973) An empirical Na-K-Ca geothermometer for natural waters. Gechemi Cosmochim Ac 37:1255–1275

Fournier RO, Truesdell AH (1974) Geochemical indicators of subsurface temperatures, 2. Estimation of temperature and fraction of hot water mixed with cold water. U.S. Geological Survey. J Res 2(3):263–269

Geological Survey of Iran (1978) Geological Map of Iran, 1:00000 Series, Sheet 5861 Avaj

Giggenbach WF (1988) Geothermal solute equilibria. Derivation of Na-K-Mg-Ca geoindicators. Geochim Cosmochim Ac 52:2749–2765

Giggenbach WF (1991) Chemical techniques in geothermal exploration. In: D'Amore F (ed) Applications of geochemistry in geothermal reservoir development. UNITAR/UNDP publication, Rome, pp 119–142

Gökgöz A, Tarcan G (2006) Mineral equilibria and geothermometry of the Dalaman–Köyceğiz thermal springs, southern Turkey. Appl Geochem 21(2):253–268

Hochstein MP, Zheng K, Pasvanoglu S, Vivian-Neal P (2013) Advective (heat sweep) geothermal systems. In Proceedings 38th workshop on geothermal reservoir engineering, Stanford University

Jackson J, Priestley K, Allen M, Berberian M (2002) Active tectonics of the South Caspian Basin. Geophys J Int 148:214–245. https://doi.org/10.1046/j.1365-246X.2002.01588.x

Karimi S, Mohammadi Z, Samani N (2017) Geothermometry and circulation depth of groundwater in Semnan thermal springs, Northern Iran. Environ Earth Sci 76(19):659

Kharaka YK, Mariner RH (1989) Chemical geothermometers and their application to formation waters from sedimentary basins. In: Naeser ND, McCulloh TH (eds) Thermal history of sedimentary basins. Springer, New York, pp 99–117

Miošić N, Samardžić N (2016) Mineral, thermal and thermomineral Waters of Bosnia and Herzegovina. In: Papic P (ed) Mineral and thermal waters of Southeastern Europe. Springer, pp 147–171

Modabberi S, Yekta SSJ (2014) Environmental geochemistry and sources of potentially toxic elements in thermal springs in the Sabalan volcanic field, NW Iran. Environ Earth Sci 71(6):2821–2835

Moeck IS (2014) Catalog of geothermal play types based on geologic controls. Renew Sustain Energy Rev 37:867–882

Mohammadi Z, Bagheri R, Jahanshahi R (2010) Hydrogeochemistry and geothermometry of changal thermal springs, Zagros region, Iran. Geothermics 39(3):242–249

Motaghi K, Shabanian E, Kalvandi F (2017) Underplating along the northern portion of the Zagros suture zone, Iran. Geophys J Int 210(1):375–389

Parkhurst DL, Appelo CAJ (1999) User's guide to PHREEQC (version2): a computer program for specia_tion, batch reaction, one_dimensional transport and inverse geochemical calculations. Water resources inves_tigations," US Geol. Surv. Rept. (95_4259)

Powell T, Cumming W (2010) Spreadsheets for geothermal water and gas geochemistry. In: Proceedings, thirty-fifth workshop on geothermal reservoir engineering, Stanford University, Stanford, California (p. 10)

Raziei T, Mofidi A, Santos JA, Bordi I (2012) Spatial patterns and regimes of daily precipitation in Iran in relation to large-scale atmospheric circulation. Int J Climatol 32(8):1226–1237

Reed M, Spycher N (1984) Calculation of pH and mineral equilibria in hydrothermal waters with application to geothermometry and studies of boiling and dilution. Geochim Cosmoch Acta 48(7):1479–1492

Ritz JF, Nazari H, Salamati R, Shafeii A, Solaymani S, Vernant P (2006) Active transtension inside central Alborz: a new insight into the northern Iran–southern Caspian geodynamics. Geology 34:477–480. https://doi.org/10.1130/G22319.1

Shamsi A, Kazemi G (2014) A review of research dealing with isotope hydrology in Iran and the first Iranian meteoric water line. Geopersia 4(1):73–86

Strelbitskaya S, Radmehr B (2010) Geochemical characteristics of reservoir fluid from NW-Sabalan geothermal field, Iran. In: Proceedings world geothermal congress, pp 25–29

Sutherland R, Townend J, Toy V, Upton P, Coussens J, Allen M, … Boles A (2017) Extreme hydrothermal conditions at an active plate–bounding fault. Nature 546(7656):137–140

Tanaka H, Chen WM, Kawabata K, Urata N (2007) Thermal properties across the Chelungpu fault zone and evaluations of positive thermal anomaly on the slip zones: are these residuals of heat from faulting? Geophy Res Lett. https://doi.org/10.1029/2006GL028153

Tester JW, Anderson BJ, Batchelor AS, Blackwell DD, DiPippo R, Drake EM, Petty S (2007) Impact of enhanced geothermal systems on US energy supply in the twenty-first century. Philos Trans A Math Phys Eng Sci 365(1853):1057–1094

Tonani F (1980) Some remarks on the application of geochemical techniques in geothermal exploration. In: Proceedings of advances in European geothermal research, 2nd symposium, Strasbourg, pp 428–443

Truesdell AH (1976) Summary of section III: geochemical techniques in exploration. In: Proceedings of the 2nd U.N. symposium on the development and use of geothermal resources, vol 1. U.S. Government Printing Office, Washington, DC, pp liii–lxxx

Yousefi H, Ehara S, Noorollahi Y (2007) Geothermal potential site selection using GIS in Iran. In: Proceedings of the 32nd workshop on geothermal reservoir engineering, Stanford University, Stanford, California, pp 174–182

Zamani H, Mahjoob M, Abadi AM (2013) The potential of using geothermal energy in Ghazvin Province, Iran. In: 2th International conference on emerging trends in energy conservation, 19–20 Feb 2013, Tehran, Iran (in Farsi)